

1 Introduction

In stretched horizontal geometries, the definition of a convenient horizontal diffusion (HD) operator is not straightforward. In this note, we present the rationale that we used to define what is the "ideal" form of a HD operator when a general stretched geometry is used; then we show that this "target" operator has a very simple form in the particular geometry of the conformal Schmidt transformation, even when coupled to the use of the spectral (Fourier-Legendre) method on the sphere, as it is the case in ARPEGE. Compared to the original HD operator (Yessad and Bénard, 1995, YB95 hereafter), this new HD operator has multiple advantages: besides its increased simplicity and cost-effectiveness, it does not suffer of any approximation, and it is much easier to tune since the total number of degrees of freedom can be brought down to two (the "global strength" and the "order" of the diffusion) for each variable to be diffused. If the second part of this work (devoted to the Schmidt transformation) is of rather particular interest, the first part (which deals with the definition of an "ideal" HD operator for stretched geometries) is of general interest for any stretched model.

2 HD operators for non-stretched geometries

The rationale to define an ideal HD operator for stretched geometries lies on the empirical observation of the way the strength of HD operators is modified when changing the resolution in models with non-stretched geometries. In a uniform geometry, the HD operator writes:

$$\frac{\partial X}{\partial t} = -K \nabla^r X, \quad (1)$$

where ∇ is the horizontal derivative operator, K is the HD coefficient, and r is the order of the HD.

The "strength" of any HD operator in a uniform resolution geometry can be quantified by the inverse of the damping time of the shortest resolved wave (the "strength" is hence denoted by τ_s^{-1} hereafter). Examination of various uniform resolution models in operation shows that when changing the resolution (i.e. Δx to fix ideas), τ_s is neither chosen proportional to Δx^r , nor independent of Δx , but rather proportional to Δx . This is due to the fact that the first (resp. second) choice is found to result into a lack (resp. an excess) of activity during the course of long integrations, especially for the smallest resolved scales. As a consequence, the HD can be written:

$$\frac{\partial X}{\partial t} = -k \Delta x^{r-1} \nabla^r X, \quad (2)$$

where the parameter k is independent of the resolution. This empirical result is thus taken as a basis to define an ideal HD operator when the resolution is not uniform, due to a stretched geometry.

3 Ideal HD operator for stretched geometries

When a stretched geometry is used, the actual horizontal coordinate (e.g. x) is replaced by a transformed coordinate $x' = f(x)$. The local map factor is then defined by $m(x) = df/dx$. The physical gradient operator $\nabla = (\partial/\partial x)$ is thus related to the transformed gradient operator $\nabla' = (\partial/\partial x')$ by: $\nabla = m \nabla'$. Let us call Δx_0 the mesh at a location where $m = 1$; we have $\Delta x = \Delta x_0/m$.

Considering the empirical observation of the previous section, the "ideal" HD operator with a stretched geometry, is the one which has everywhere the same properties as for a non-stretched geometry with the same local resolution. Hence, the ideal HD operator must write:

$$\frac{\partial X}{\partial t} = -k \Delta x^{r-1} \nabla^r X = -k \Delta x_0^{r-1} m^{1-r} \nabla^r X. \quad (3)$$

Generally, the HD operator of the stretched model is rather specified in terms of the transformed derivative operator ∇' :

$$\frac{\partial X}{\partial t} = -k \Delta x_0^{r-1} m \nabla'^r X. \quad (4)$$

It is worth noting that in (3) and (4), the parameter k is by nature independent of the space, but also of the absolute resolution Δx_0^{-1} . As a consequence, for a given transformation f , k does not need to be changed when increasing the resolution of the model. The parameter k is said space- and resolution-independent.

4 Particular case of Schmidt transformation

The stretched ARPEGE model uses a particular analytical stretching transformation proposed by Schmidt (1977) which allows an algebraic treatment of the equations in the stretched geometry, coupled with the spectral method. Let θ be the latitude on the non-stretched sphere, and Θ the latitude on the stretched sphere. We note $\xi = \sin \Theta$. The ARPEGE stretching transformation is defined by:

$$\theta(\xi) = \arcsin \left(\frac{a\xi + b}{a + b\xi} \right), \quad (5)$$

where $a = (c^2 + 1)/2c$ and $b = (c^2 - 1)/2c$ and c is the stretching factor. The local map factor is given by:

$$m(\xi) = \frac{\partial \Theta}{\partial \theta} = a + b\xi. \quad (6)$$

The original HD operator of ARPEGE (see YB95) consisted in a mixture of a pure ∇'^r operator and an approximated $\nabla^u = m^u \nabla'^u$ operator:

$$\frac{\partial X}{\partial t} = -K m \nabla'^r X - K_u \widehat{m}^u \nabla'^u X, \quad (7)$$

where \widehat{m}^u is a second-degree approximation of m^u given by:

$$\widehat{m}^u = a_0 + a_1 \xi + a_2 \xi^2. \quad (8)$$

It appears clearly from (7) and (4) that doing $K = 0$, $u = r$, $a_0 = a$, $a_1 = b$ and $a_2 = 0$, the original ARPEGE HD operator can be transformed into the ideal HD operator defined in the previous section. The advantages of this approach are multiple: (i) the HD operator becomes tri-diagonal in the spectral space instead of penta-diagonal (see YB95); (ii) the obtained HD operator is exactly the ideal one, instead of an approximation of it; (iii) by writing $K_u = k \Delta x_0^{r-1}$ the obtained HD coefficient k can be shown to be space-, resolution-, and stretching-independent. This latter property is important since any change in the geometry can be done without retuning the HD coefficient k , which was not true with the original ARPEGE HD operator defined in YB95.

5 Conclusion

The work presented here allows to rationalize the formulation of HD operators for models with stretched horizontal geometries. For any of these models, an ideal HD operator can be found, allowing the definition of a space- and resolution-independent parameter k . For the special case of the Schmidt stretching transformation, the algebraic nature of the transformation makes it possible to obtain a HD coefficient which is additionally stretching-independent. This new HD operator has been implemented operationally in ARPEGE since february 2003.

References

- Schmidt, F., 1977: Variable fine-mesh in spectral global model *Beitr. Phys. Atmosph.*, **50**, 211-227.
- Yessad, K., and P. Bénard, 1995: Introduction of a local mapping factor in the spectral part of the Météo-France global variable mesh numerical forecast model. *Q. J. Roy. Met. Soc.*, **122**, 1701-1719.

Stable algorithms for the NH version of the LAM "Aladin"

PIERRE BÉNARD*, JOZEF VIVODA⁺, PETRA SMOLIKOVÁ[†], JAN MASEK⁺

* *Centre National de Recherches Météorologiques, Météo-France, Toulouse, France*

⁺ *Slovak Hydro-Meteorological Institute, Bratislava, Slovakia*

[†] *Czech Hydro-Meteorological Institute, Prague, Czech Republic*

1 Introduction

In the last issue of this JSC/CAS WGNE report we stated, according to theoretical analyses, that even when choosing "optimal" prognostic nonhydrostatic variables, the classical semi-implicit (SI) scheme suffers from a lack of robustness for Euler Equations in presence of mesoscale features (steep orography, strong nonlinearities,...), and that more sophisticated time-discretisations are required in order to achieve a robustness compatible with the use of semi-Lagrangian (SL) schemes in these circumstances. These previous conclusions are confirmed here by adiabatic numerical experimentation performed with the nonhydrostatic (NH) version of the Aladin limited-area model.

2 ICI schemes

In order to remove the instabilities linked to explicitly treated terms, an Iterative Centred-Implicit (ICI) scheme has been implemented in Aladin-NH in addition to the move from the original (d) prognostic variable to the "optimal" variable (d') as described in the last issue. The principle of this ICI scheme is to approach the centred-implicit solution by an iterative method. Let the meteorological system to be solved write symbolically as:

$$\frac{\partial \mathcal{X}}{\partial t} = \mathcal{M}.\mathcal{X}. \quad (1)$$

The proposed ICI time-discretisation is defined for the iteration index n as follows: (e.g. for a 2 time-level (2-TL) discretisation):

$$\frac{\mathcal{X}^{+(n)} - \mathcal{X}^0}{\Delta t} = \frac{\mathcal{M}.\mathcal{X}^{+(n-1)} + \mathcal{M}.\mathcal{X}^0}{2} + \frac{\mathcal{L}^*.\mathcal{X}^{+(n)} - \mathcal{L}^*.\mathcal{X}^{+(n-1)}}{2} \quad (2)$$

for $n = 1, 2, \dots, N_{\text{iter}}$, where \mathcal{L}^* is a linear operator, and the traditional superscript NWP notation for time levels is adopted (+ for time $(t + \Delta t)$, and 0 for time t). In this generalised fixed-point algorithm conditioned by \mathcal{L}^* , the initial guess $\mathcal{X}^{+(0)}$ is arbitrary as well as the \mathcal{L}^* operator. However, since \mathcal{L}^* acts as a conditioner, an inappropriate choice of \mathcal{L}^* may prevent the convergence of the algorithm. The choice of $\mathcal{X}^{+(0)}$ is less crucial, but a non-extrapolating $\mathcal{X}^{+(0)} = \mathcal{X}^0$ choice may enhance the stability (see Cullen, 2000). The final \mathcal{X}^+ state, valid at $(t + \Delta t)$ is then taken as the last iterated state $\mathcal{X}^{+(N_{\text{iter}})}$ where N_{iter} is an arbitrary number. When the convergence is achieved (which implies $N_{\text{iter}} = \infty$), the obtained scheme is a Centred-Implicit scheme, which can be expected to be very robust.

The analysis of the behaviour of ICI schemes in terms of stability can be performed using similar techniques as in Simmons et al. 1978 for the SI scheme (see e.g. Bénard, 2003). When the scheme is unstable, increasing the number of iterations may increase the growth-rate since the iterative process then becomes divergent. However, the domain of stability of the ICI scheme is generally found wider than for the SI scheme, which justifies its use as an alternative.

In practice, N_{iter} is chosen very small in order to keep an acceptable efficiency. We use the following choices: $\mathcal{X}^{+(0)} = \mathcal{X}^0$, $N_{\text{iter}} = 2$, and \mathcal{L}^* is the same operator as for the classical SI algorithm (defined by $N_{\text{iter}} = 1$). Since only one additional iteration is performed compared to the SI algorithm, this scheme is referred to as "predictor/corrector" (PC) scheme, the SI iteration being the predictor substep and the additional iteration being the corrector one.

3 Results

Extensive testing have been performed to confirm the theoretical statements found by analysis. Two main type

of experiments are reported here: academic 2D orographic flows, and adiabatic real-data 3D flow, drawn from the PYREX field-experiment.

For the 2D academic flows, we chose to present a non-hydrostatic non-linear regime characterized by the following settings: smoothly varying hybrid η coordinate, 128 point horizontal extension with $\Delta x = 200\text{m}$, 100 levels with a regular $\Delta z = 300\text{m}$, Agnesi orography with height $h = 1000\text{m}$ and half-width $a = 1000\text{m}$. The initial thermal profile has a surface temperature $T_s = 293\text{K}$, a uniform Brunt-Vaisala frequency $N = 0.01\text{ s}^{-1}$ up to 12000m, and is isothermal above. The wind is uniform $V = 10\text{ m.s}^{-1}$, and the sea-level pressure is $\pi_s = 1013.25\text{ hPa}$. For the definition of the \mathcal{L}^* operator, uniform reference values $T^* = 220\text{K}$ and $\pi_s^* = 900\text{hPa}$ are chosen. A smooth sponge is applied in the stratosphere, and the time-step is $\Delta t = 5\text{s}$ for the 3-TL SI SL scheme, and $\Delta t = 10\text{s}$ for the 2-TL PC SL (non-extrapolating) scheme. No diffusion or decentering is applied. The stability of the experiments is summarized in Table 1, where the number of completed time-steps is indicated for each configurations.

	3-TL SI	2-TL PC
d	55	20
d'	stable	stable

Table 1: number of completed time-steps for 2D experiments.

It should be noted that the 2-TL PC scheme is more unstable than the 3-TL SI scheme in the first line, reflecting a divergence in the iteration process. The advantage of the PC scheme does not appear explicitly in this table since the move to d' is sufficient to stabilize the system. However, in other 2D configurations, a clear advantage is observed to the PC scheme (see also 3D case below).

For the 3D experiments, the configuration is as follows: 277×181 horizontal points with $\Delta x = 2635\text{m}$, and 41 levels with a hybrid η coordinate. The initial state is drawn from the PYREX field-experiment data-set, and consists in a strong flow over Pyrénées mountains. A moderate horizontal diffusion (but no decentering) is applied, and the time-step is $\Delta t = 15\text{s}$ for the 3-TL SI SL scheme, and $\Delta t = 30\text{s}$ for the 2-TL PC SL (non-extrapolating) scheme. The stability of the experiments is summarized in Table 2, where the number of completed time-steps is indicated for each configurations.

	3-TL SI	2-TL PC
d	83	13
d'	281	stable

Table 2: number of completed time-steps for 3D experiments.

This configuration, close to a future operational target, shows a clear advantage to the combination of d' with a PC scheme.

4 Conclusion

The results are consistent with theoretical statements which were indicating that the classical SI scheme is not robust enough for solving the Euler equations in strongly non-linear regimes, even with an appropriate choice for the set of prognostic variables. The use of more sophisticated ICI schemes allows to remedy to the weaknesses of the SI scheme. It should be noted that the computational cost of the ICI schemes is proportional to N_{iter} , hence this class of scheme has a practical interest only for very low values of N_{iter} . Specifically, 2-TL PC and 3-TL SI schemes have the same computational cost if the time-step of the 2-TL scheme is twice the one of the 3-TL scheme. However, in the case where the physical parameterisation package is computationally expensive (as it will be increasingly the case for mesoscale applications), there is an additional significant advantage to the PC scheme in term of computational cost since most of the physical parameterisations should be called only once per time-step.

References

- Bénard, P., 2003: Stability of Semi-Implicit and Iterative Centred-Implicit Time Discretisations for Various Equation Systems Used in NWP. Submitted to *Mon. Wea. Rev.* (available on request at: pierre.benard@meteo.fr)
- Cullen, M. J. P., 2000: Alternative implementations of the semi-Lagrangian semi-implicit schemes in the ECMWF model. *Q. J. R. Meteorol. Soc.*, **127**, 2787-2802.
- Simmons, A. J., B. Hoskins, and D. Burridge, 1978: Stability of the semi-implicit method of time integration. *Mon. Wea. Rev.*, **106**, 405-412.

ICON: Development of an icosahedral, non-hydrostatic global model

*L. Bonaventura, M. Giorgetta, I. Kirchner,
L. Kornbluh, D. Majewski, A. Müller,
A. Rhodin, B. Ritter, E. Roeckner* *

Max Planck Institut für Meteorologie
Bundesstraße 55, 20146, Hamburg, Germany

and

Deutscher Wetterdienst
Frankfurter Str. 135, 63067, Offenbach, Germany

The German Weather Service - Deutscher Wetterdienst (DWD) and the Max Planck Institute for Meteorology (MPI) have started the development of a new GCM, including a new gridpoint dynamical core based on a icosahedral spherical grids, within the ICON (ICOsahedral Non-hydrostatic) project.

MPI has developed in the past general circulation models for climate research applications, the latest being ECHAM5. The ECHAM dynamics is solved by the spectral transform method following the ECMWF implementation. This method is still very successful when applied to the dynamics of the atmosphere, but it has displayed several inconveniences when coupled to the simulation of conserved or long-lived chemical constituents of air. Furthermore, application to stratospheric and higher atmospheric studies are gaining increasing importance within the research plans of MPI and their optimal development would also profit from a general reformulation of the available models.

DWD operates the German weather forecast system from the global to the regional scale. The current global model, GME (see e.g. [4]), operates entirely in grid point space using a triangulated icosahedral grid. This development has been driven by the idea that the impact of localized atmospheric forcing related to detailed land characteristics on the circulation is modelled more accurately in grid point space models than in spectral transform models. Furthermore, the icosahedral grid approach allows a quasi uniform coverage of the sphere. DWD intends to include more detailed physical processes and a more detailed coupling of the atmosphere to the surface, specifically to the ocean surface. Furthermore, there is a desire to integrate the current global and local forecasting systems in a unique model with a local grid refinement capability.

The project has started in May 2002 and the new complete model should be available by the end of 2005. Various universities and research institutions have joined the project and a more complete description is available at <http://icon.enes.org>.

* Corresponding author, e-mail: roeckner@dkrz.de

The ICON model is being designed to employ a set of fully compressible, non-hydrostatic equations. Many standard meteorological approximations, e.g. constant acceleration of gravity, constant distance from the Earth's center, neglection of the Coriolis terms associated with the vertical velocity, which are not motivated by clearcut computational advantages or by theoretical analysis, will be avoided. The continuity equation will be formulated in flux form and the total density of air will be considered as the prognostic variable in the continuity equation, along with the baricentric velocity of air and of the moist species.

A prototype shallow water model is under development, starting with a basic second order discretization of the vector invariant form of the shallow water equations on a C-grid staggered variable arrangement on both the hexagonal and triangular icosahedral grids, along the lines of a semi-implicit extension of [3]. A mass conservative formulation of the continuity equation is employed and compatibility with later three-dimensional extensions of the horizontal discretization approach is going to be ensured. Semi-lagrangian schemes will also be employed in the final implementation. Other efficient higher order methods (discontinuous Galerkin, spectral finite volume) will also be considered, along with mass conservative local grid refinement options. The different discretization options are being compared and evaluated on the standard test case suite (see e.g. [5]). A prototype, x-z two-dimensional nonhydrostatic model will also be developed. Various choices of coordinate transformations will be compared, including hybrid terrain following height coordinate, hybrid isentropic coordinates and natural height based coordinates, without terrain following normalization. Efficient higher order methods (discontinuous Galerkin, spectral finite volume) will also be considered. Special effort will be devoted to include in the model the local computation of a well balanced hydrostatic state at each time step along the lines of [2]. This may possibly lead in the complete model to the intermediate computation of a three-dimensional state in geostrophic and hydrostatic balance. The different discretization options will be evaluated on appropriate test case suites (see e.g. [1]).

References

- [1] L. Bonaventura. A semi-implicit, semi-lagrangian scheme using the height coordinate for a nonhydrostatic and fully elastic model of atmospheric flows. *Journal of Computational Physics*, 158:186–213, 2000.
- [2] N. Botta, R. Klein, S. Langenberg, and S. Lützenkirchen. Well balanced finite volume methods for nearly hydrostatic flows. *Journal of Computational Physics*, to appear, 2002.
- [3] Shian-Jiann Lin and Richard B. Rood. An explicit flux-form semi-Lagrangian shallow water model on the sphere. *Quarterly Journal of the Royal Meteorological Society*, 123:2477–2498, 1997.
- [4] Detlev Majewski, Dörte Liermann, Peter Prohl, Bodo Ritter, Michael Buchhold, Thomas Hanisch, Gerhard Paul, Werner Wergen, and John Baumgardner. The operational global icosahedral-hexagonal gridpoint model GME: description and high resolution tests. *Monthly Weather Review*, 130:319–338, 2002.
- [5] David L. Williamson, John B. Drake, James J. Hack, Rüdiger Jakob, and Raul N. Swarztrauber. A standard test set for numerical approximations to the shallow water equations in spherical geometry. *Journal of Computational Physics*, 102:221–224, 1992.

Preserving long-term accuracy in semi-implicit schemes for slightly compressible flow

Michael J.P. Cullen

Department of Mathematics, University of Reading, Reading U.K. RG6 6AX

m.j.p.cullen@reading.ac.uk

Semi-lagrangian methods for passive advection problems have the advantage that accuracy is maintained over a full timestep; since the equations are integrated along characteristics. The same applies to characteristic-based upwind Eulerian methods. In Riemann-solver based methods for compressible flows, accuracy is again maintained by transporting appropriate variables along the characteristics of the system.

In incompressible flows, this property will only be maintained if the trajectories describe a volume-preserving mapping from particle positions at departure points to their positions at arrival points, (Cullen 2002 section 3). No attempt is normally made to enforce this, since it requires implicit calculation of the departure points. The errors resulting from this can be calculated by diagnosing the flow Jacobian:

$$J = \det \frac{\partial(x_d, y_d, z_d)}{\partial(x_a, y_a, z_a)} \quad (1)$$

where suffices a and d refer to arrival and departure points respectively. Experiments in the model of Smolarkiewicz et al. (1999), reported by Cullen et al. (2001), showed that there could be substantial errors of up to 28% in a single time-step where the trajectories were deflected by orography.

In an incompressible problem, the errors can be reduced by iterative recalculation of the departure points. For a slightly compressible problem, the relevant case for the atmosphere, the equivalent procedure is to solve the continuity equation in Lagrangian form as

$$\rho_a = \rho_d J \quad (2)$$

where J is given by (1). This can be proved by arguments similar to Cullen and Maroofi (2001). This equation has to be solved implicitly for numerical stability. We achieve this by using a predictor-corrector method, Cullen (2001). For example, for the calculation of the x -coordinate of the departure points, this gives

$$x_a = x_d^* + (u_d^t + u_a^t)\delta t; \quad x_a = x_d + (u_d^t + u_a^*)\delta t \quad (3)$$

In our implementation, J is approximated by finite differences. This is straightforward in either two or three dimensions. In schemes designed to ensure formal conservation, e.g. Zerroukat et al. (2002), J has to be calculated by defining a departure-point control volume and integrating all variables over it. This is much harder in three dimensions than in two.

We demonstrate the viability of the method by using a slice version of the Met Office non-hydrostatic Unified Model (Cullen et al. 1997). The approximation to J is chosen so that the scheme is equivalent to the standard scheme in the limit of small timesteps. We solve a problem of flow at 10ms^{-1} over periodic hills of height 2000m and wavelength 5km. A 40×40 mesh is used. Since the scheme is equivalent to the standard scheme for short timesteps, we assess the relative performance by calculating the sensitivity to time step length. The table shows the r.m.s differences between various quantities between Courant numbers of 0.2 and 0.4; and between 0.4 and 0.8. Two versions of the model are compared:

A: Standard scheme with semi-Lagrangian advection of density and Ritchie method of calculating departure points.

B: Predictor-corrector scheme with solution of (2).

The table shows r.m.s differences calculated at two times. The first time is during the transient stage when the flow is being set up. The later time is when the steady state is being approached.

Table 1: Test of integration schemes.

Scheme/test	r.m.s. θ	rms u	rms w	r.m.s. θ	rms u	rms w
A .2/.4	.0180	.0142	.1324	.0343	.0212	.0408
B .2/.4	.0030	.0043	.0689	.0053	.0188	.0291
A .2/.8	.0283	.1535	.2477	.0855	.1099	.0951
B .2/.8	.0292	.0502	.2019	.0256	.0817	.1257

The results comparing the shorter timesteps show that the predictor-corrector scheme B gives much less timestep sensitivity than scheme A especially with shorter timesteps and integration periods. Plots of the results show that the results change substantially between Courant numbers of 0.4 and 0.8, so the differences may be less reliable than for the shorter timestep comparison. Experiments were also carried out with the predictor-corrector scheme using the standard form of the continuity equation and semi-lagrangian advection of density. This combination was found to be unstable, suggesting that (2) may be more robust than the standard formulation..

As used here, scheme B is twice as expensive as A. It is, however, likely that the cost of B could be substantially reduced by rationalising the iterations in the Helmholtz solver and the departure point calculations. Cullen (2001) showed that the predictor-corrector scheme (without the use of the Lagrangian continuity equation (2)) could be cost-effective in the ECMWF model. These results suggest that the same may apply to the Met Office model.

References

- CULLEN,M.J.P., DAVIES,T., MAWSON,M.H., JAMES,J.A. and COULTER,S. (1997) An overview of numerical methods for the next generation UK NWP and climate model. in 'Numerical Methods in Atmosphere and Ocean Modelling'. The Andre Robert Memorial Volume. (C.Lin, R.Laprise, H.Ritchie, Eds.), Canadian Meteorological and Oceanographic Society, Ottawa, Canada, pp 425-444.
- CULLEN,M.J.P. (2001) Alternative implementations of the semi-Lagrangian semi-implicit scheme in the ECMWF model. *Quart. J. Roy. Meteorol. Soc.*, **127**, 2787-2802.
- CULLEN,M.J.P. and MAROOFI, H. (2001) The Fully Compressible Semi - Geostrophic System from Meteorology. *Arch. Rat. Mech. Anal.*, accepted.
- CULLEN,M.J.P., SALMOND,D.J. and SMOLARKIEWICZ,P.K., (2001) Key numerical issues for the future development of the ECMWF model. In Proc. 2000 Workshop on 'Developments in numerical methods for very high resolution global models', ECMWF, Reading, UK, pp 183-206.
- CULLEN,M.J.P. (2002) New mathematical developments in atmosphere and ocean dynamics, and their application to computer simulations. in 'Large-scale atmosphere-ocean dynamics', vol.1, J.Norbury and I.Roulstone eds., Cambridge University Press, pp 202-287.
- SMOLARKIEWICZ,P.K., GRUBIVSIC,V., MARGOLIN,L.G. and WYSZOGRODSKI,A.A. (1999) Forward-in-time differencing for fluids: Nonhydrostatic modelling of fluid motions on a sphere. In Proc. 1998 Seminar on 'Recent Developments in Numerical Methods for Atmospheric Modelling', ECMWF, Reading, UK, pp 21-43.
- ZERROUKAT,M., WOOD,N. and STANIFORTH,A. (2002) SLICE: A semi-lagrangian inherently conserving and efficient scheme for transport problems. *Quart. J. Roy. Meteorol. Soc.*, **128**, 2801-2820.

HIGHER ORDER FINITE DIFFERENCE SCHEMES FOR ADVECTION OF NHM

FUJITA Tsukasa

Numerical Prediction Division / Japan Meteorological Agency

1-3-4 Otemachi, Chiyoda-ku, Tokyo 100-8122, JAPAN

fujita@met.kishou.go.jp

The nonhydrostatic model (NHM) of JMA, which has been developed for the very short-range prediction of rainfall, has been used mainly with a second-order finite difference scheme (Ishida 2001; Fujita *et al.* 2002). Two types of higher-order accurate schemes are implemented and tested. Since flux form equations are employed in NHM (Saito *et al.* 2001), the straightforward second order stencil is defined as

$$\frac{\partial U\theta}{\partial x} = \frac{(U\bar{\theta})_{i+1/2} - (U\bar{\theta})_{i-1/2}}{\Delta x},$$

where overbars denote horizontal interpolation. Higher-order schemes are derived referring wider range in the same direction. A fourth-order scheme is written as follows.

$$\frac{\partial U\theta}{\partial x} = \frac{9}{8} \frac{(U\bar{\theta})_{i+1/2} - (U\bar{\theta})_{i-1/2}}{\Delta x} - \frac{1}{8} \frac{(U\bar{\theta})_{i+3/2} - (U\bar{\theta})_{i-3/2}}{3\Delta x}$$

In the above equation interpolation processes should be done with high-order accuracy to guarantee the accuracy of the stencil, and the divergence term should be also computed accurately to keep conservation property in the isentropic case. Third- and fifth-order schemes require interpolation for not only θ , but also U . The third-order scheme is defined as follows.

$$\frac{\partial U\theta}{\partial x} = \frac{1}{12\Delta x} \left\{ (U\bar{\theta})_{i-3/2} - 18(U\bar{\theta})_{i-1/2} + 8(\bar{U}\theta)_i + 9(U\bar{\theta})_{i+1/2} \right\}$$

Truncation errors of the schemes above are smaller than the counterparts of the schemes in unstaggered coordinate, and subsequently the dispersive and diffusive effect of the staggered schemes is smaller.

Alternative schemes, which are used in WRF (Wicker and Skamarock 2002), are derived by considering numerical fluxes through the cell interfaces. A fourth-order scheme is defined as follows.

$$\frac{\partial U\theta}{\partial x} = \frac{F_{i+1/2}^{4th} - F_{i-1/2}^{4th}}{\Delta x} \quad \text{where} \quad F_{i-1/2}^{4th} = \frac{U_{i-1/2}}{12} \{7(\theta_i + \theta_{i-1}) - (\theta_{i+1} + \theta_{i-2})\}$$

The accuracy of this scheme is guaranteed when the flow field is uniform. Schemes of different accuracy are constructed in a similar manner. These schemes will be called 'Cell Interface Difference' (CID) in this manuscript.

Figure 1 shows results of a comparison experiment of realistic simulations by NHM. The model is initialized at 00 UTC December 4, 2002, and run with 10 km horizontal resolution over the eastern part of Japan. The second-order scheme produces short-wave structures in the accumulated rainfall field, while the third-order scheme gives a smooth distribution mainly due to the numerical diffusion implied in the difference scheme. The fourth-order staggered scheme also yields a smoother field than the second-order, which suggests the higher-order scheme affects the prediction by the less dispersive characteristic. The high-order interpolation implied in the stencils may also have an effect on the fields to some extent. In the meantime, large-scale fields such as the sea level pressure field

are not distinctively different. The results of the CID schemes hold similar property, however, the fourth-order CID yields not as smooth an accumulated rainfall field as the counterpart of the staggered scheme. The reason of the difference may be attributed to the difference of the actual order of accuracy between the two schemes and the effect of interpolation implied in the staggered scheme.

The computational costs of the higher-order schemes in elapse time were compared, and the results almost justified elimination of the third-order staggered scheme from the choices since it was more costly than the fourth-order staggered scheme, and as costly as the fifth-order staggered scheme. The larger cost of the third-order staggered scheme perhaps comes from the extra interpolation cost for U . The CID schemes work economically since interpolation cost is minimized in the stencil and high-order treatment for the divergence term is unnecessary.

Overall, the fourth-order staggered scheme is favored for the coming operational run of NHM, and the fourth-order CID may be an alternative.

REFERENCES

- Ishida, J., 2001: Development of the operational non-hydrostatic model at the Japan Meteorological Agency. *DWD Forschung und Entwicklung, Arbeitsergebnisse*, **68**.
- Fujita, T., K. Saito, Y. Yamada, J. Ishida, M. Narita, S. Goto, C. Muroi, T. Kato, and H. Eito, 2002: Development of a nonhydrostatic model for very short-range forecasting at JMA. *15th Conf. on Numerical Weather Prediction*, San Antonio, TX, Amer. Meteor. Soc., 13.3.
- Saito, K., T. Kato, E. Hisaki, and C. Muroi, 2001: Documentation of the Meteorological Research Institute / Numerical Prediction Division unified nonhydrostatic model. *Tec. Rep. MRI*, **42**, 133 pp.
- Wicker, L. J., and W. C. Skamarock, 2002: Timesplitting method for elastic models using forward time schemes. *Mon. Wea. Rev.*, **130**, 2088-2097.

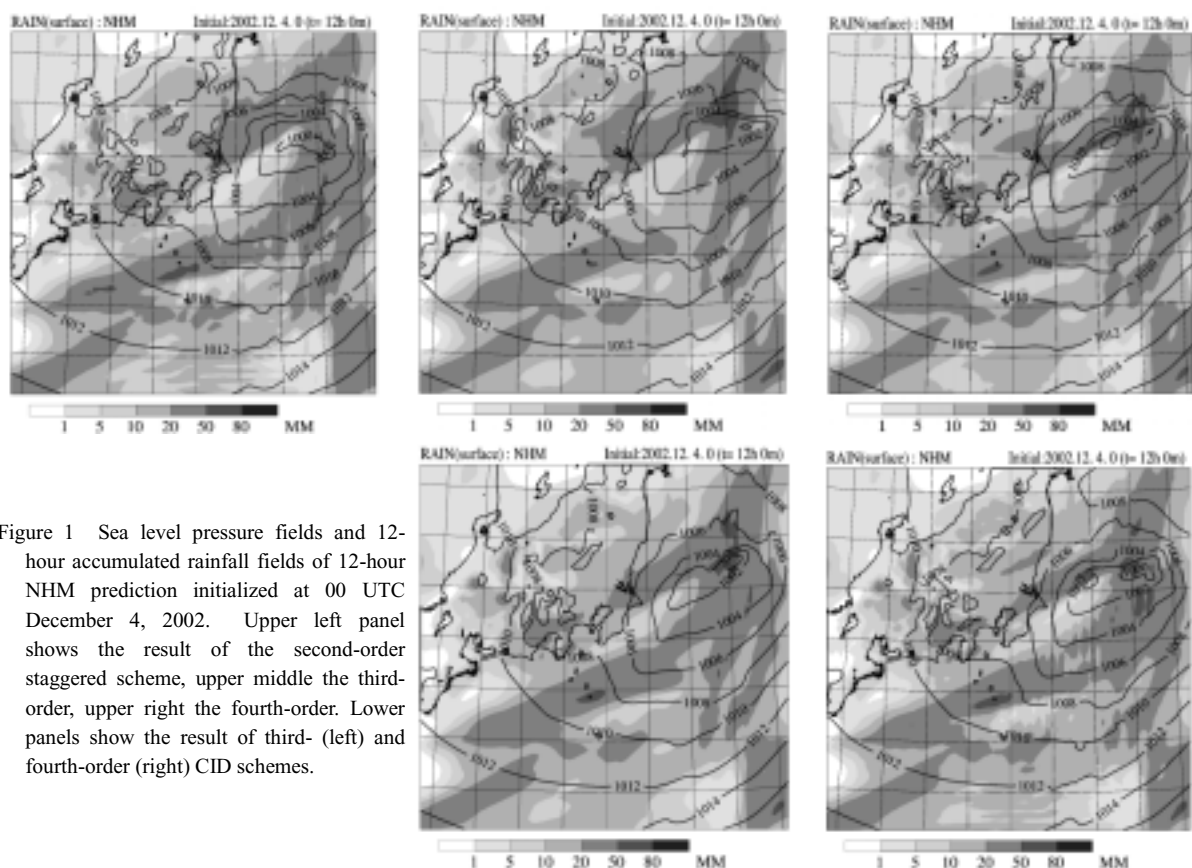


Figure 1 Sea level pressure fields and 12-hour accumulated rainfall fields of 12-hour NHM prediction initialized at 00 UTC December 4, 2002. Upper left panel shows the result of the second-order staggered scheme, upper middle the third-order, upper right the fourth-order. Lower panels show the result of third- (left) and fourth-order (right) CID schemes.

Development of a 20 km mesh global NWP model on the Earth Simulator

Keiichi Katayama*, Hiromasa Yoshimura** and Takayuki Matsumura*

*Numerical Prediction Division, Japan Meteorological Agency

**Climate Research Department, Meteorological Research Institute

e-mail: k-katayama@naps.kishou.go.jp

1) Introduction

The Japan Meteorological Agency (JMA) has been operating a MPI parallel version of a T213L40 global spectral model (GSM) which corresponds to a 60 km mesh model. GSM supports the official one-week forecast and provides the lateral boundary condition for the JMA Regional models. In order to provide finer scale forecast, we are developing a very high resolution GSM which corresponds to a 20 km mesh global model.

In the summer of 2002, the researcher groups of the Numerical Prediction Division (NPD/JMA) and the Meteorological Research Institute (MRI) got computer accounts from the Earth Simulator Center to study the global warming with super high resolution atmospheric models on the world fastest supercomputer "Earth Simulator" (ES).

The global modeling groups of NPD/JMA and the Climate Research Department of MRI have developed a new global model which is called "JMA-MRI unified global model". The features of this model are Fortran90 coding style, a new semi-Lagrangian scheme and some new physical schemes. We are testing this new model as the next JMA operational global model (TL319L40). We are also trying to execute a very high resolution global model such as TL1023L40 20 km mesh model on the ES.

2) Development on the ES

The ES is the world's fastest supercomputer. Its peak performance is 40Tflops. The ES is a distributed memory parallel computer system which consists of 640 processor nodes. Each processor node is a shared memory system which contains 8 vector processors. Its operating system software and compilers are almost same as NEC-SX series supercomputers. The MPI library is used for inter-node parallelization, and microtasking, which is shared memory parallel programming, is used for intra-node parallelization in our global model. In order to get a high performance, it is necessary to make some program tuning both for vector processing and for microtasking. Automatic vectorization and parallelization are applied by the Fortran90 compiler, but we need to rewrite some codes and/or insert some directive lines manually for full optimization. Current performance of our global model is 18% of the peak performance.

3) 20km mesh global model

Several experimental runs of T682L40 20km mesh global model was executed on the JMA supercomputer system (Hitachi SR8000E1). We have been trying to run TL1023L40 semi-Lagrangian 20km mesh global model on the ES. The horizontal grid space of TL1023L40 is 2048x1024. The elapse time of 1 day forecast is about 2 hours on 8 nodes of the ES. We are trying to execute the TL1023L40 model on 100-200 nodes. Figure 1 shows a forecast example of TL1023L40. The spiral cloud patterns around typhoons and the small scale clouds on the Tibetan plateau are well simulated in the TL1023L40 20 km mesh model.

4) Future plans

We will continue to optimize the JMA-MRI unified global model to get the best performance on the ES. The JMA operational global model will change to TL319L40 semi-Lagrangian model in 2003. It is expected that the semi-Lagrangian GSM which corresponds to 20 km mesh resolution will be executed on the next JMA supercomputer system in 2006.

TL1023L40 Typhoon forecast (09 Jul 2002 00UTC, FT=24, GMS-IR forecast images)

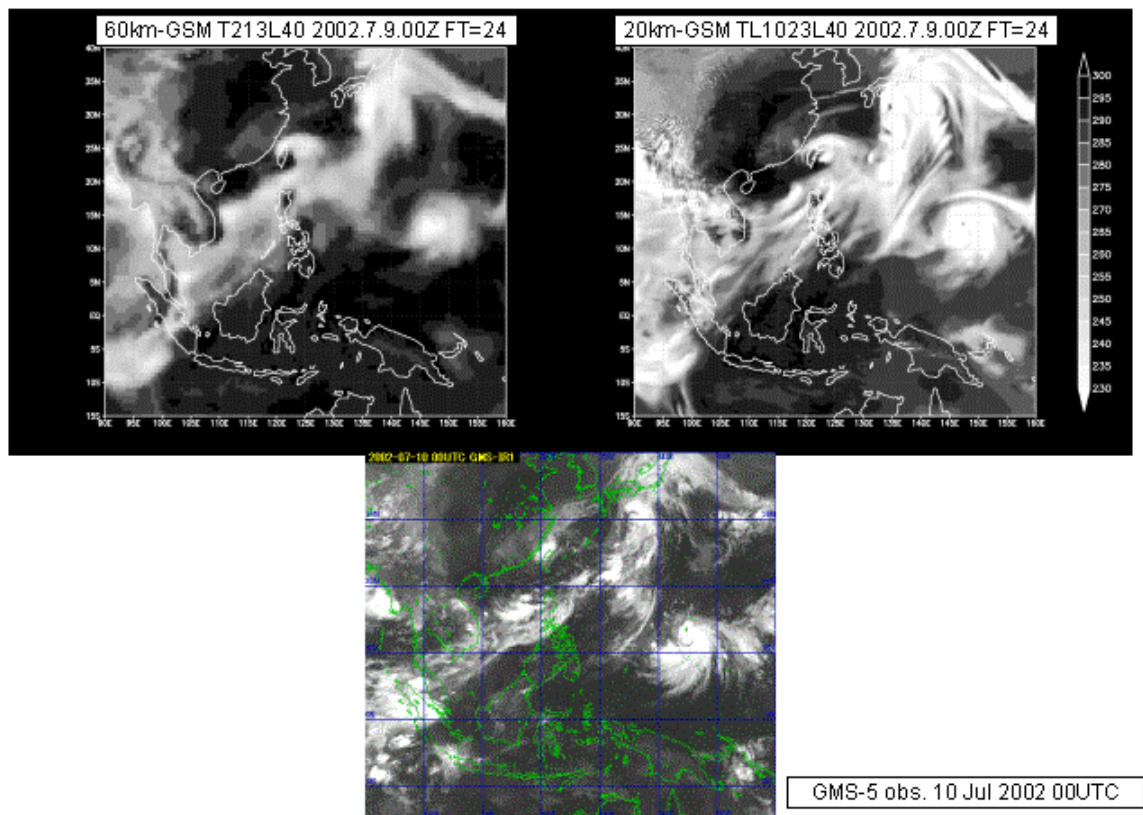


Fig.1 Forecast cloud images of T213L40 (upper left), TL1023L40 (upper right) and observation by GMS-5 (lower).

A generalized hybrid transformation for tracer advection

W. J. Merryfield, N. McFarlane, and M. Lazare

Canadian Centre for Climate Modelling and Analysis, Meteorological Service of Canada, University of Victoria, Victoria, B.C., Canada email: *Bill.Merryfield@ec.gc.ca*

Atmospheric and ocean circulation models often advect variables that vary rapidly in space or have a very large dynamical range. Examples include moisture and chemical species in atmospheric models, and chloroflourocarbons and biogeochemical tracers in ocean models. Such variables present a challenge for numerical advection algorithms, which often produce artificial extrema or “fill in” deep minima. Undesirable side effects include unphysical negative values of chemically active tracers, spurious moisture saturation leading to unphysical precipitation, and an unrealistically shallow stratospheric moisture minimum.

Efforts to overcome these difficulties typically have focused on improving spatial resolution or employing more sophisticated (and inevitably more expensive) advection algorithms. Here we describe a transformed variable approach that enables improvement to be attained without such measures. Under this approach, the quantity that is advected is a transformed variable s that is related to the physical variable q by

$$s = \frac{q_0}{[1 + p \ln(q_0/q)]^{1/p}}, \quad q < q_0, \quad (1)$$
$$s = q, \quad q \geq q_0,$$

where q_0 and p are constants. This is a generalization of the hybrid transformation proposed by Boer (1995), for which $p = 1$.

Figure 1 illustrates use of the transformation in a simple one-dimensional advection problem. The advected function has steep gradients and a dynamic range of 10^4 , about that of moisture between the troposphere and lower stratosphere. The function has been advected across one cycle of a periodic domain, consisting of 128 grid points. Two advection algorithms are considered. For the numerically diffusive upstream method (left), the transformation improves representation of the minimum and sharp edges. Even more dramatic improvement is realized for spectral advection (right), where, as in some circulation models, modest explicit dissipation has been added to reduce Gibbs fringes.

An obvious hazard is that advection of q becomes non-conservative, even when s is globally conserved. An error analysis indicates that when the leading spatial truncation error is of second order, as for both algorithms considered above, the rate of nonconservation scales as

$$\frac{\partial}{\partial t} \int q(\mathbf{x}, t) d\mathbf{x} \propto \int \frac{\partial q}{\partial s} \frac{\partial^2 s}{\partial x^2} d\mathbf{x}. \quad (2)$$

When considered as a function of (q_0, p) this rate is generally positive for $q_0 \lesssim \max(q)$ and negative for $q_0 \gtrsim \max(q)$, as in Fig. 2, where the left-hand panel shows (2) evaluated for exact $q(x)$ in Fig. 1, and the right-hand panel accumulated nonconservation for the computation in Fig. 1b. Separating these regimes is a locus of exact global conservation of q ; in the Fig. 1 examples, (q_0, p) were chosen to conserve q to within 0.1%. Though the nonconservation rate depends also on the spatial distribution of q , its main features as illustrated in Fig. 2 are not strongly dependent on the function being advected.

Transformation (1) has been tested for spectral advection (with weak dissipation) of moisture and chemical species in the CCCma developmental atmospheric general circulation model AGCM4, with (q_0, p) tuned to maintain near-conservation of these variables. Moisture nonconservation rates as percentages of precipitation, indicated for various (q_0, p) in Fig. 2b taking $\max(q)=20\text{g/kg}$, exhibit similar trends to those in the 1d example.

Because of nonconservation issues, the technique described here is not suitable for applications where exact advective conservation of tracers is essential. However, in instances where tracer inventories are established by balances between sources and sinks rather than a memory of initial conditions, the method may provide a useful means for enhancing the fidelity of a given advection algorithm.

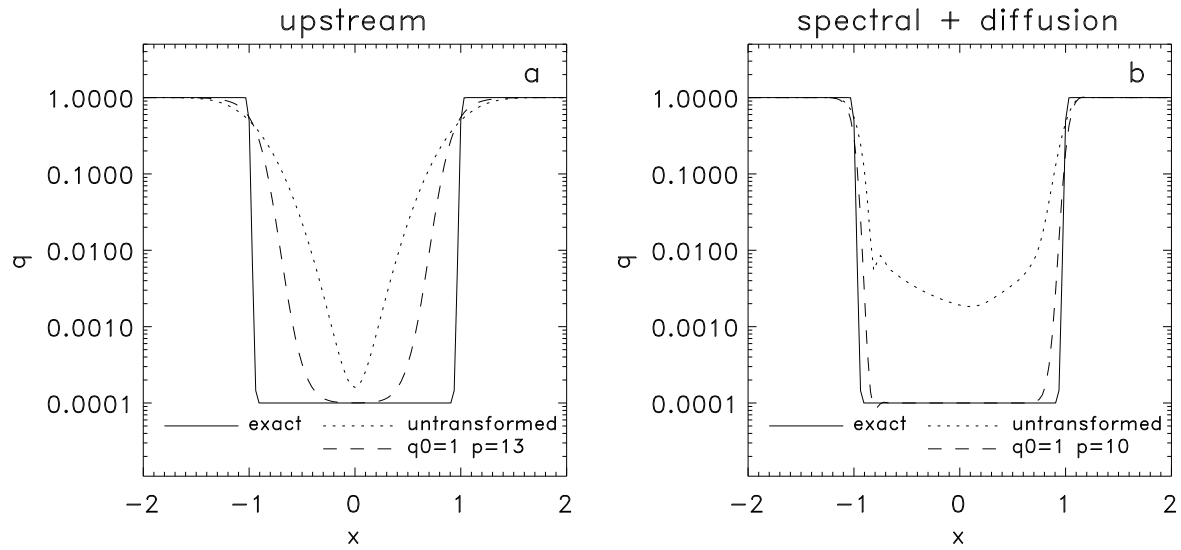


Figure 1: Advection of a 1d function through one cycle of a periodic domain, using transformed and untransformed variables: (a) upstream method; (b) spectral advection with explicit diffusion.

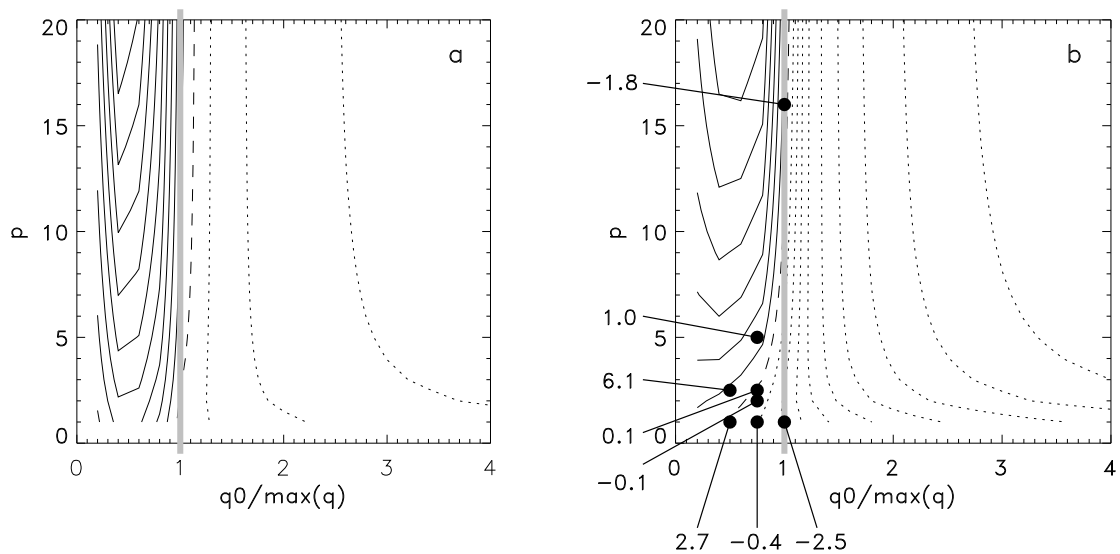


Figure 2: Contours of q nonconservation corresponding to Fig. 1b: (a) as calculated from (2) for exact $q(x)$; (b) as deduced numerically. Solid contours are positive and dotted contours are negative; the zero contour is dashed. Nonconservation rates for moisture in a 3d GCM are indicated in (b).

Reference

Boer, G.J., 1995: A hybrid moisture variable suitable for spectral GCMs. *Research Activities in Atmospheric and Oceanic Modelling. Report No. 21*, WMO/TD-No. 665, World Meteorological Organization, Geneva.

Time-splitting of advection in the JMA Nonhydrostatic Model

Kazuo Saito

Numerical prediction Division, 1-3-4 Otemachi, Chiyoda-ku, Tokyo 100-8122, Japan
ksaito@npd.kishou.go.jp

The Japan Meteorological Agency (JMA) started an operational run of a 10 km horizontal resolution mesoscale NWP model in March 2001. The model, MSM, is a high-resolution version of the JMA's operational regional spectral model, where the hydrostatic equilibrium is assumed. As for its initialization, mesoscale 4DVAR has been introduced in March 2002. Meanwhile, JMA will replace MSM with a nonhydrostatic model in March 2004. Development of an operational nonhydrostatic model for regional NWP (NHM) has been underway, based on the Meteorological Research Institute/Numerical Prediction Division unified nonhydrostatic model (MRI/NPD-NHM; Saito et al., 2001; <http://www.mri-jma.go.jp/Dep/fo/mrinpd/INDEXE.htm>).

Among the three dynamical cores of MRI/NPD-NHM, the split-explicit time integration scheme (HE-VI scheme) is used for operation, considering the computational efficiency on the distributed memory parallel computer in the JMA's NWP system. The HE-VI scheme of MRI/NPD-NHM treats sound waves in the short time step, but has no special treatment for gravity waves. For operational purpose, it is crucial to stabilize the gravity wave modes and remove the dependency of the maximum time step on the atmospheric static stabilities.

Saito (2002) proposed a time splitting scheme of gravity waves for NHM where the computation of the buoyancy terms and vertical advection of the reference potential temperature are treated in the short time step in the HE-VI scheme. This scheme stabilizes the gravity waves, however, in case horizontal wind is strong, it is not necessarily effective to use a large time step in the leap-frog time integration. A new time splitting scheme of advection has been developed to improve the computational stability of NHM.

In the HE-VI scheme of NHM, the forward time integration

$$\frac{U^{\tau+\Delta\tau} - U^{\tau}}{\Delta\tau} + \frac{\partial P^{\tau}}{\partial x} + \frac{\frac{1}{G^2} \partial_z^* P^{\tau}}{G^2 \partial_z^*} = -(ADVU + RU), \quad (1)$$

$$\frac{V^{\tau+\Delta\tau} - V^{\tau}}{\Delta\tau} + \frac{\partial P^{\tau}}{\partial y} + \frac{\frac{1}{G^2} \partial_z^* P^{\tau}}{G^2 \partial_z^*} = -(ADV V + RV), \quad (2)$$

are used for horizontal momentums, and the backward time integration

$$\frac{W^{\tau+\Delta\tau} - W^{\tau}}{\Delta\tau} + \frac{1}{mG^2} \frac{\partial P^{\beta}}{\partial z^*} + \frac{g}{mC_m^2} P^{\beta} = \frac{1}{m} BUOY - (ADV W - RW), \quad (3)$$

$$\frac{P^{\tau+\Delta\tau} - P^{\tau}}{\Delta\tau} + C_m^2 (-PFT + m^2 (\frac{\partial U^{\gamma}}{\partial x} + \frac{\partial V^{\gamma}}{\partial y})) + m \frac{\partial}{\partial z^*} [\frac{1}{G^2} \{W^{\beta} + m(G^{\frac{1}{2}} G^{13} U^{\gamma} + G^{\frac{1}{2}} G^{23} V^{\gamma})\}] - PRC = dif.P, \quad (4)$$

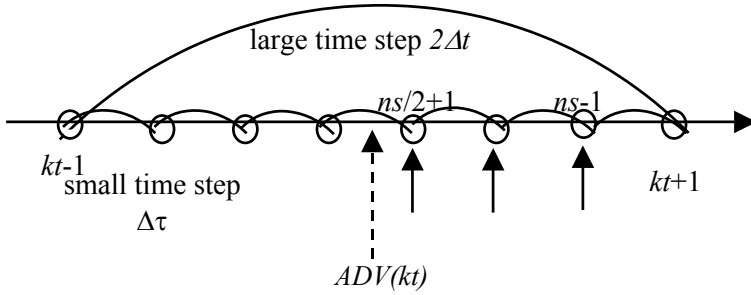
are employed for vertical momentum and pressure. In NHM, advection terms are originally computed in the long time step Δt . It is expected that computing advection terms in short time step $\Delta\tau$ contributes to improve the computational stability. However, this choice is not acceptable because the higher order

advection scheme with the modified scheme is expensive and spoils the merit of HE-VI scheme.

In the new splitting scheme, we fully evaluate higher-order advection terms with the modified scheme at the center of the leap-frog time step, and then adjust the lower-order (second-order) components at each short time step in the later half of the Leap-frog time integration as

$$ADV = ADV(kt) - ADVL(kt) + ADVL^\tau. \quad (5)$$

Here, $ADV(kt)$ is the higher order advection with the modified scheme at time step kt , $ADVL(kt)$ and $ADVL$ is the lower-order advection component at kt and each short time step $\Delta\tau$, respectively. This adjustment is done from $(ns-1)/2+1$ to $ns-1$, where ns is the ratio of $2\Delta t$ and $\Delta\tau$.



Time splitting of advection terms. Case of $ns = 7$.

In order to split the gravity waves, equations for the potential temperature and vertical momentum are rewritten as

$$\frac{\theta^{\tau+\Delta\tau} - \theta^\tau}{\Delta\tau} = -(ADV\theta - ADVL\theta + ADVL\theta^\tau) + \frac{Q}{c_p\pi} + dif.\theta = ADVL\theta - ADVL\theta^\tau + \left[\frac{\partial\theta}{\partial t} \right], \quad (6)$$

$$\begin{aligned} \frac{W^{\tau+\Delta\tau} - W^\tau}{\Delta\tau} + \frac{1}{mG^{\frac{1}{2}}} \frac{\partial P^\beta}{\partial z^*} + \frac{g}{mC_m^2} P^\beta = \frac{1}{m} \frac{\rho G^{\frac{1}{2}} \theta^{\tau+\Delta\tau} (1 + 0.61Q_v)(1 - Q_c - Q_r - Q_i - Q_s - Q_g)}{\theta_m} g \\ - (ADVW - ADVLW + ADVLW^\tau - RW). \end{aligned} \quad (7)$$

As in Saito (2002), the third term of *r.h.s.* of (6) is given by a tentative time integration in the cloud microphysical process.

This time splitting scheme enables the model to use 40 sec. for Δt of the leap-frog scheme in the simulation of 10 km horizontal resolution, which (roughly speaking) corresponds to 80 sec. in the second order Runge-Kutta time integration scheme. Additional computational cost for time splitting of advection is less than 10 % of the total computation time when the model includes cloud microphysics.

References.

- Saito, K., 2002: Time-splitting of gravity waves in the Meteorological Research Institute/Numerical Prediction Division unified Nonhydrostatic Model. *CAS/JSC WGNE Research Activities in Atmospheric and Oceanic Modelling*, **32**, 0321-0322.
- Saito, K., T. Kato, H. Eito and C. Muroi, 2001: Documentation of the Meteorological Research Institute/Numerical Prediction Division unified nonhydrostatic model. *Tech. Rep. MRI*, **42**, 133pp.

Variable resolution version of the SL-AV global NWP model

Mikhail Tolstykh

*Institute of Numerical Mathematics, Russian Academy of Sciences,
and Russian Hydrometeorological Research Center
9/13 B. Predtezenskii per., 123242 Moscow RUSSIA
email:tolstykh@rhmc.mecom.ru*

Russia is stretched along longitude, and most part of it is located north from the 50 degree latitude. As the meridians of the spherical coordinate converge towards the poles, the longitudinal resolution increases while approaching the pole. A model on the latitude-longitude grid with variable resolution in latitude can provide local increase of resolution in this area by a factor of 2.2 with respect to the constant resolution version without significant deformation of the horizontal grid. This increase can be achieved at virtually no cost.

The SL-AV is a global semi-Lagrangian NWP model [1]. This model uses the absolute vorticity as a prognostic variable and compact high-order finite differences on the unstaggered grid. A detailed description of the numerics for the 2D version of the model is given in [2]. The model includes the parameterization package of subgrid-scale processes from the French operational model ARPEGE/IFS [3].

The variable resolution in latitude is implemented by introduction of an auxiliary coordinate (pseudolatitude) with constant step. The partial derivative in latitude of some function can be written as

$$\frac{\partial f}{\partial \varphi} = \frac{\partial \varphi'}{\partial \varphi} \frac{\partial f}{\partial \varphi'}$$

where φ' is pseudolatitude, and $\frac{\partial f}{\partial \varphi'}$ is discretized as in the case of constant resolution. All derivatives in this expression are discretized with the fourth order accuracy.

This approach was tested with the set of twelve 5-day forecasts starting at 15th day of each month 1996, 0000 UTC. The initial data were uninitialized ECMWF analyses (truncated to T119 spectral resolution). Digital filter initialization was applied. The resolution was 1.40625 degrees in longitude, 28 irregularly spaced σ -levels and the time step was equal to 36 min. The resolution in latitude as a function of grid point number is depicted in Fig. 1. The high resolution (≈ 75 km) zone is placed between 30 and 90 N. The ratio between the adjacent mesh intervals does not exceed 1.065.

On Fig. 2 we present averaged over 12 cases RMS errors for 500, 850 hPa heights and mean sea-level pressure (MSLP) for the 50N-90N band for constant resolution (1.125 degrees) and variable resolution versions of the model.

It is known that the variable grid strategy is limited to the relatively short-range forecasts, since for medium-range forecasts, the high resolution region will come under influence of weather systems that at initial time are far away, and hence are poorly resolved in the analysis. Indeed, one can see that the variable resolution version is more accurate than constant resolution one up to approximately 84 hours range. At the same time, the RMS errors for ranges up to 72 hours are better by 1-2 m. The improvement is more visible in skill score S1 (not shown).

The plans include the increase in horizontal resolution and also testing a configuration with rotated poles and variable resolution.

This work was supported by the RFBR grant 01-05-64582.

References

- [1] M.A. Tolstykh, Semi-Lagrangian high resolution model of the atmosphere for numerical weather prediction, *Russian Meteorology and Hydrology*, N4, 1-9 (2001). (Russian and English)
- [2] M. Tolstykh, Vorticity-divergence semi-Lagrangian shallow-water model on the sphere based on compact finite differences, *J. Comput. Phys.* **179** (2002), 180-200.

- [3] J.-F. Geleyn, E. Bazile, P. Bougeault *et al*, Atmospheric parameterization schemes in Meteo-France's ARPEGE N.W.P. model. In *Parameterization of subgrid-scale physical processes*, ECMWF Seminar proceedings (1994), 385-402.

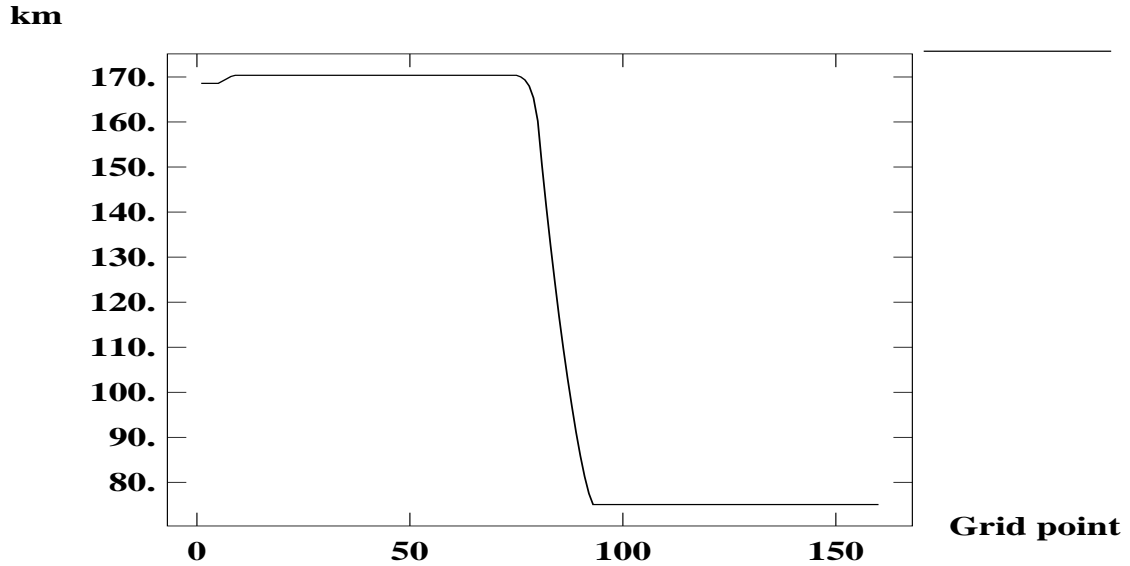


Figure 1: The latitudinal resolution as a function of gridpoint number. (from Southern pole to Northern pole)

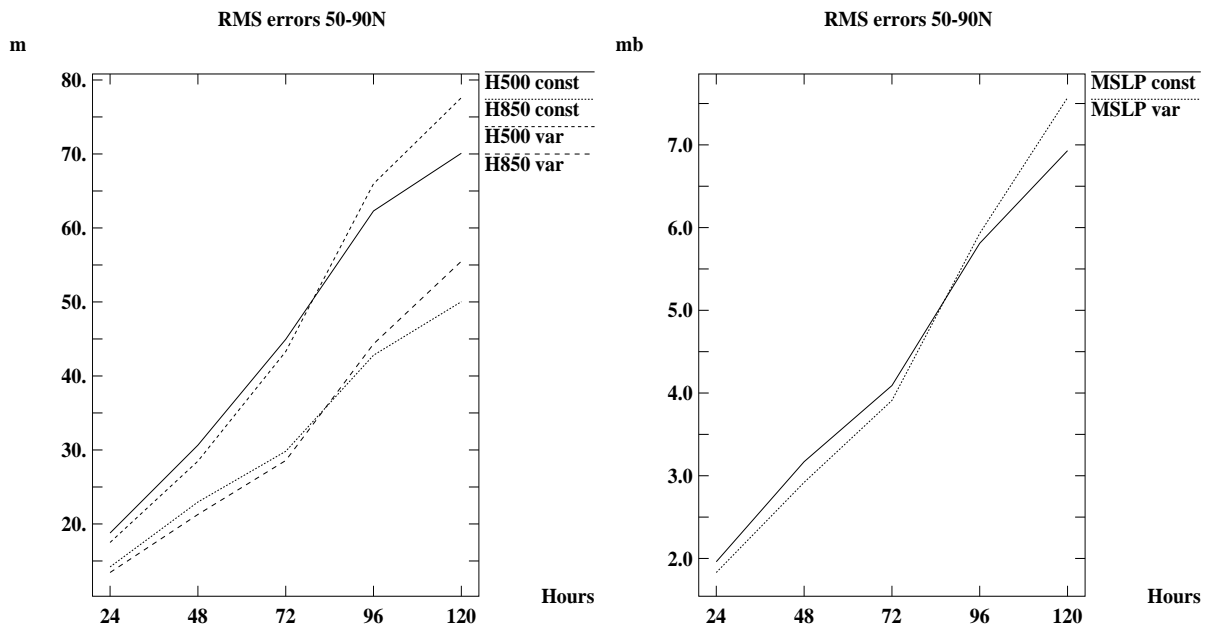


Figure 2: The averaged RMS errors of 500 and 850 hPa heights (left) and mean sea-level pressure (right) as functions of the forecast time.

A Semi-Lagrangian Scheme Conservative in the Vertical Direction

Hiromasa Yoshimura

Climate Department, Meteorological Research Institute, Japan Meteorological Agency
E-mail: hyoshimu@mri-jma.go.jp

Takayuki Matsumura

Numerical Prediction Division, Japan Meteorological Agency

1. Introduction

The conservation of a semi-Lagrangian advection scheme is a considerable issue for a climate model. We develop a new semi-Lagrangian scheme for a climate model with a conserving property in vertical advection.

2. The semi-Lagrangian advection scheme conservative in the vertical direction

In the new semi-Lagrangian advection scheme, computation of the advection terms is split into the horizontal and vertical directions and the both terms are computed separately. The flux in the vertical direction is evaluated with a one-dimensional conservative semi-Lagrangian scheme, while the horizontal advection is calculated with a conventional non-conservative 2-dimensional semi-Lagrangian scheme. Note that we can conserve mass and water vapor when we adopt a correction method such as Gravel et al. (1994). The new advection scheme also has the advantage of computational efficiency, since it reduces the number of spatial interpolation.

The continuity equation is

$$\frac{\partial}{\partial t} \left(\frac{\partial p}{\partial \sigma} \right) + \mathbf{v}_H \cdot \nabla_H \left(\frac{\partial p}{\partial \sigma} \right) + \frac{\partial}{\partial \sigma} \left(\frac{\partial p}{\partial \sigma} \right) = 0, \quad (2.1)$$

and the moisture equation is

$$\frac{\partial}{\partial t} q + \mathbf{v}_H \cdot \nabla_H q + \frac{\partial}{\partial \sigma} q = 0, \quad (2.2)$$

where p is the pressure, q is the mixing ratio of water vapor, \mathbf{v}_H is the horizontal wind vector and σ is the hybrid vertical coordinate of p and $\sigma (= p/p_s)$.

From (2.1) and (2.2) we obtain

$$\frac{d_H}{dt} \left(\frac{\partial p}{\partial \sigma} \right) = \left(\mathbf{v}_H \cdot \nabla_H \right) \left(\frac{\partial p}{\partial \sigma} \right) + \frac{\partial}{\partial \sigma} \left(\frac{\partial p}{\partial \sigma} \right), \quad (2.3)$$

$$\frac{d_H}{dt} \left(\frac{\partial p}{\partial \sigma} q \right) = \left(\mathbf{v}_H \cdot \nabla_H \right) \left(\frac{\partial p}{\partial \sigma} q \right) + \frac{\partial}{\partial \sigma} \left(\frac{\partial p}{\partial \sigma} q \right). \quad (2.4)$$

In (2.3) and (2.4), the term on the left hand side $d_H/dt = \partial_H/\partial t + \mathbf{v}_H \cdot \nabla_H$ is the horizontal part of the advection, the first term on the right hand side is the divergence and the second term on the right hand side is the vertical flux.

The discrete analogs of (2.3) and (2.4) are

$$\frac{d_H}{dt} (\sigma p_k) = \left(\mathbf{v}_H \cdot \nabla_H \right)_k (\sigma p_k) + \frac{\partial}{\partial \sigma} \left(\frac{\partial p}{\partial \sigma} \right)_{k+1/2}, \quad (2.5)$$

$$\frac{d_H}{dt} (\sigma p_k q_k) = \left(\mathbf{v}_H \cdot \nabla_H \right)_k (\sigma p_k q_k) + \frac{\partial}{\partial \sigma} \left(\frac{\partial p}{\partial \sigma} q \right)_{k+1/2}, \quad (2.6)$$

where k is the vertical level.

We integrate (2.3) and (2.4) in time in the order as follows:

- The divergence at the departure point at time ($t - \Delta t$)
- The vertical flux at the departure point at time ($t - \Delta t$)
- The horizontal advection (with a conventional 2-dimensional semi-Lagrangian scheme)
- The vertical flux at the arrival point at time ($t + \Delta t$)
- The divergence at the arrival point at time ($t + \Delta t$)

The flux of the water vapor in the vertical direction is evaluated with a one-dimensional conservative semi-Lagrangian scheme.

The advection terms of the moisture equation should be computed consistently with that of the continuity equation. In normal semi-Lagrangian schemes, only the continuity equation is split to compute its advection terms and this may cause inconsistency between mass and other non-split variables such as water vapor. In this report we split the advection terms of the moisture equation and compute them in a similar manner to the continuity equation, ensuring the consistency on treatment of advection between the continuity and the moisture equations. The advectons of the temperature and the horizontal wind components are also computed in the same way as the water vapor.

3. 3-years runs at the resolution T42L40

We performed three 3-years runs at the resolution T42L40 and compared the results. One of three was an Eulerian advection scheme, another one was a conventional semi-Lagrangian advection scheme (Matsumura 2002), and the last one was the vertically conservative semi-Lagrangian advection scheme proposed here.

In both semi-Lagrangian schemes, a time step Δt is set to 45 min, which is about twice as long as that determined by the Courant number.

Results of the 3-years runs are summarized as follows:

- With respect to the 3-years average (i.e. climate), cooling bias appears around the tropical tropopause in the conventional semi-Lagrangian scheme (Fig. 1), while it does not in the vertically conservative semi-Lagrangian scheme (Fig. 2).
- The amount of the false heat source in the atmosphere, which is calculated from the difference between the 3-years average of the total energy flux at the top and the one at the bottom, is smallest in the vertically conservative semi-Lagrangian scheme. This means that the vertically conservative semi-Lagrangian scheme is best among the three with respect to the conserving property of energy.
- In the 24-hours forecast, the difference of sea level pressure between the two semi-Lagrangian schemes is small.

These results show that the vertically conservative semi-Lagrangian scheme is better than the conventional semi-Lagrangian scheme for a long-term integration.

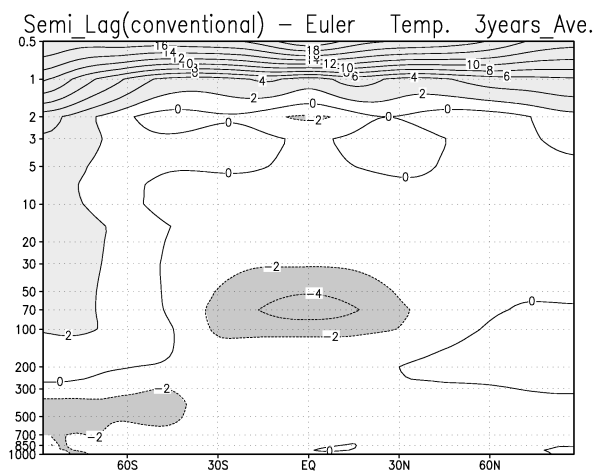


Fig. 1. The zonal mean temperature difference between the conventional semi-Lagrangian scheme and the Eulerian scheme.

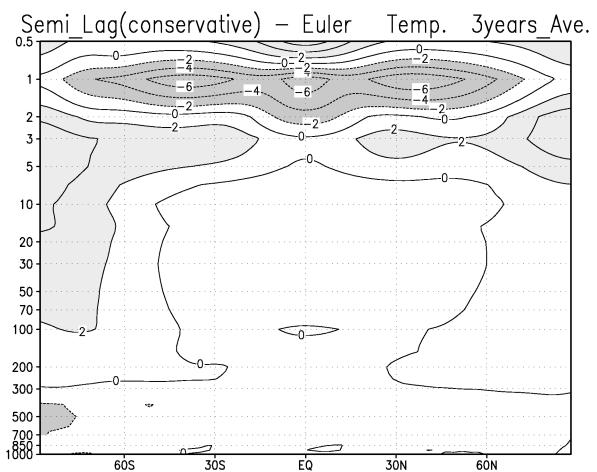


Fig. 2. The same as Fig. 1 except between vertically conservative semi-Lagrangian scheme and the Eulerian scheme.

A new interpolation method for high frequency forcing fields

Jorge Zavala-Hidalgo¹, Peng Yu, Steven L. Morey, Mark Bourassa, and James J. O'Brien

Center for Ocean-Atmospheric Prediction Studies, The Florida State University

A new generation of very high-resolution ocean numerical models allows the study of processes close to the inertial frequency and even in superinertial frequencies. These processes require that the models be forced by high frequency forcing fields, which in many cases are obtained from atmospheric numerical models, typically in 6 hourly fields. These fields commonly represent the values of surface fluxes of wind stress, evaporation, precipitation, and heat fluxes at the specified date and time instead of averages for a given period. Oceanographers usually linearly interpolate these fields in time to the model time step. This is a good approximation for features that behave like standing waves, i.e., change their amplitude without displacement. When there are strong moving features, such as fronts, the interpolated fields behave like duplicated standing fronts changing their amplitude instead of moving. Here, a new technique for the interpolation of the forcing fields in time that recovers the movement of features is tested in a simple case. This method decomposes the fields into their complex empirical orthogonal functions, then the information from each mode is used to interpolate in time and finally the significant modes are added. This technique is a particular case of the time and space interpolation that is currently applied to altimetry data at the Center for Ocean-Atmospheric prediction Studies (Yu et al., 2003).

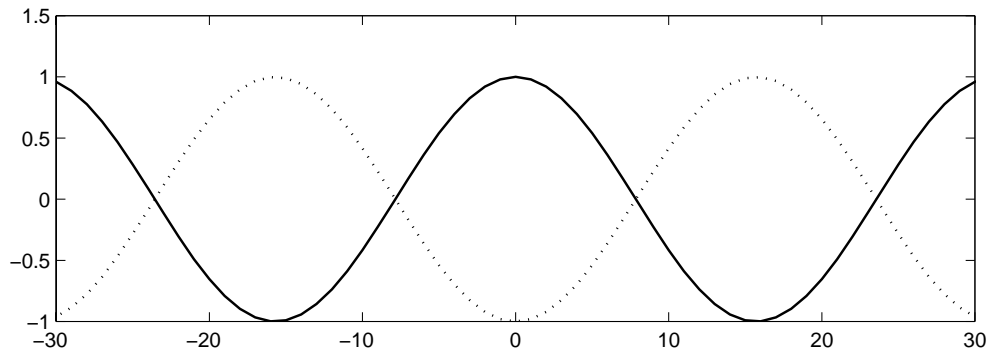


Figure 1. Position of the synthetic feature at time $t = 0$ (continue line), and at time $t = 1$ (dotted line). The abscissa axis is the distance in arbitrary units and the ordinate axis is the amplitude.

A moving feature defined by a cosine shape moving to the right illustrates the technique (Fig. 1). A standard weighted linear interpolation between two sampled fields shows that the feature in the interpolated field changes its amplitude, duplicates, and does not translate in space. In contrast, with the new technique, the amplitude has a smaller variation, and the feature translates (Fig. 2).

¹ zavala@coaps.fsu.edu

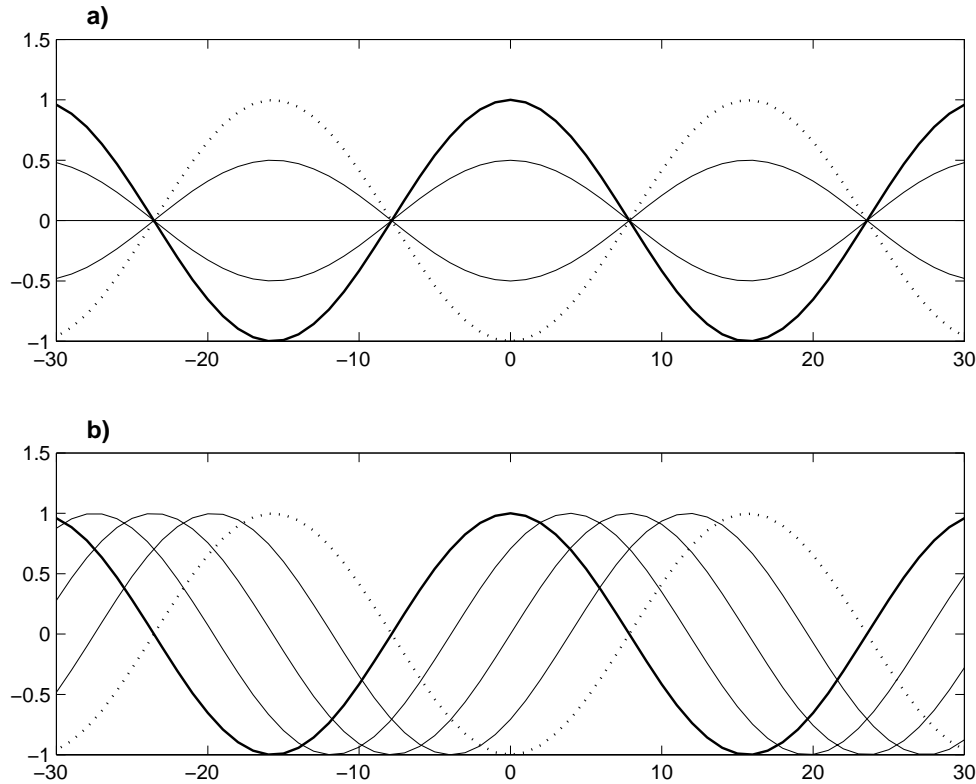


Figure 2. Position of the feature between two sampled times interpolated by a) weighted linear interpolation and b) the complex empirical orthogonal function interpolation method. The thick and dotted lines represent the position of the wave at time $t = 0$ and $t = 1$ respectively, and the thin lines represent the estimated positions at times $t = 1/4$, $t = 1/2$, and $t = 3/4$.

A generalization of this technique is being developed and applied to the high frequency forcing fields used to force the COAPS/Florida State University Gulf of Mexico simulation (Morey et al., 2003).

Acknowledgments. The Center for Ocean-Atmospheric Prediction Studies receives its base funding from ONR Secretary of the Navy Grant to James J. O'Brien, the NASA Physical Oceanography Program and through the Applied Research Center, funded by NOAA Office of Global Programs.

References

- Morey, S. L., P. J. Martín, J. J. O'Brien, A. A. Wallcraft, and J. Zavala-Hidalgo: Export pathways for river discharge fresh water in the northern Gulf of Mexico. Submitted to *J. Geophys. Res.*, 2003.
- Yu, P., J. Zavala-Hidalgo, J. J. O'Brien, A new gridding method for satellite altimeter data, Research Activities in Atmospheric and Ocean Modeling, CAS/JSC Working Group on Numerical Experimentation, 2003.